Data-Driven Neuroendocrine-PID Controller Design for Twin Rotor MIMO System

Data-Driven Neuroendocrine-PID Controller Design for Twin Rotor MIMO System

M.R. Ghazali, M.A. Ahmad and R.M.T. Raja Ismail
Instrumentation & Control Engineering Research Group (ICE), Faculty of Electrical & Electronics Engineering, Universiti Malaysia Pahang, 26600 Pekan, Pahang, Malaysia.

E-mail: riduwan@ump.edu.my

Abstract. This paper presents the design of a data-driven neuroendocrine-PID controller based on adaptive safe experimentation dynamics (ASED) method for a twin-rotor MIMO system (TRMS). Neuroendocrine-PID is deemed a compatible controller, often due to its biological-inspired mechanism from a human's endocrine system that promotes control effectiveness and accuracy. In assessing the robustness of the proposed controller, its parameters were optimized through the ASED method, by tracking both error and input control performances. In particular, the ASED method is a game-theoretic method that randomly perturbs several elements of its controller parameters to search for the optimal controller parameters. Comparison was further made alongside performance of a standard PID controller. Following the simulation conducted, findings with regards to total norm error and total norm input have hereby suggested neuroendocrine-PID as a better controller, following a 13.2% improvement in control accuracy to that of a standard PID controller for TRMS system.

1. Introduction

Complex nonlinear MIMO systems have been widely studied within multiple engineering applications, in view of modelling, controlling and optimizing. In particular, the Twin Rotor MIMO system (TRMS) which replicates a helicopter-based dynamics, constitutes heightened nonlinearity, following exceptional coupling effect of the pitch and yaw angle of the system. It, thus, requires the implementation of controller structures, with the like of PID controller [1, 2, 3], H_∞ controller [4], Linear Quadratic (LQ) controller [5], Fuzzy controller [6], Fuzzy-PD controller [7], sliding mode control [8], fuzzy sliding mode controller [9] etc.; towards gauging the desired positions alongside the compatible control signals.

In conjunction, evolutionary techniques, such as PSO, GSA, GA, etc., are further being integrated within controller structures in tuning the necessary parameters [1, 2, 3, 6]. Within this context, initial techniques are often based upon multi-agent optimizations, which accounts for population-based searches that adopt large group of agents over an immersive set of feasible solutions. With agent-to-agent interactions in seek of an optimal solution, greater dimensions of design parameters would require an extensive computation interval; thus, lesser time efficiency. Such downfall is overcome by single solution optimization methods, such as simultaneous perturbation stochastic approximation (SPSA) [10, 11], Simulated Annealing [12], safe experimentation dynamics (SED) [13, 14], adaptive safe experimentation dynamics (ASED) [15], and random search (RS) [16]. Improvement is hereby achieved through modifying single candidate solution based on random perturbation of design parameters, further maintaining

a comparatively shorter computation interval within the design process of single-agent based optimizations.

Moreover, nature-inspired controllers, specifically within the aspect of biological phenomena, have also been designed within the area of nonlinear MIMO systems, including the neuroendocrine-PID controller[17]. As such, neuroendocrine-PID has been proposed by [13, 18] alongside sigmoid based secretion rate neuroendocrine-PID within the application of a container gantry crane system. The potential of this controller should not be overlooked, typically in attaining greater control performance accuracy. Through the integration of neuroendocrine, enhancement is achieved via improved efficiency and control performance, which surpasses that of a standard PID controller.

With regards to the fore-discussed areas, this paper explores the fundamental of neuroendocrine within system control, by presenting neuroendocrine-PID as the controller for nonlinear TRMS systems. Herewith, Adaptive Safe Experimentation Dynamics (ASED) optimization has then been applied to tune the controller's parameters. Being a single-agent method towards attaining optimal design parameters, ASED is foregrounded for its ability in providing stable convergence, while acquiring better control accuracy by retaining the best optimal values when the parameters are being updated. Additionally, it adapts to the system's objective function, further prevents the issue of premature convergence during updating of the design parameters [15]. With this, effectiveness of ASED has been showcased, towards acquiring optimal parameters for the proposed neuroendocrine-PID controller, which entails better control performance.

In this case, two main aspects were being evaluated in assessing performance of the proposed controller, namely tracking error and control input energy. With ASED as the underpinning basis for parameter optimization, this research contributes through verifying the robustness of neuroendocrine-PID towards enabling a more superior control performance accuracy to that of a standard PID.

Explicitly, this paper is organized into five main sections, as follows: The first section covers an introduction to the current study; whereas, the second section provides explanations on the investigated TRMS system, along with problem formulation on the proposed neuroendocrine-PID based upon the data-driven scheme. Next, the third section illustrates design of the proposed controller with integration of ASED as its optimization approach. Robustness of the proposed controller is then validated within a TRMS system, as presented in the fourth section. It is hereby placed in comparison against a standard PID for the purpose of determining performance superiority. Last but not least, a thorough conclusion for this paper is presented in the fifth section.

Notation: The real number sets and the positive real number sets are denoted separately via $\mathbb{R}$ and $\mathbb{R}_+$. The set of n real number is represented by the symbol $\mathbb{R}^n$. $\mathbf{0}$ and $\mathbf{1}$ are hereby defined as the vector in which all elements are zero and one, respectively.

2. Problem Formulation

For this section, the Twin Rotor MIMO system (TRMS) system as emphasized within this study is firstly explained; followed by the problem setting of the proposed neuroendocrine-PID as the controller for the investigated system. Herewith, a TRMS with its main and tail propellers being independently driven by DC motors has been studied [19], as illustrated in Fig. 1. The system's outputs are denoted by a_h and a_v at horizontal and vertical planes, respectively. Whereas, the voltage inputs for the DC motors at the main and tail propellers are denoted by u_h and u_v. With this, the dynamic equations of TRMS are given as:

$$\dot{s_h} = l_t S_f F_h(\omega_t) \cos a_v - k_h \Omega_h, \tag{1}$$

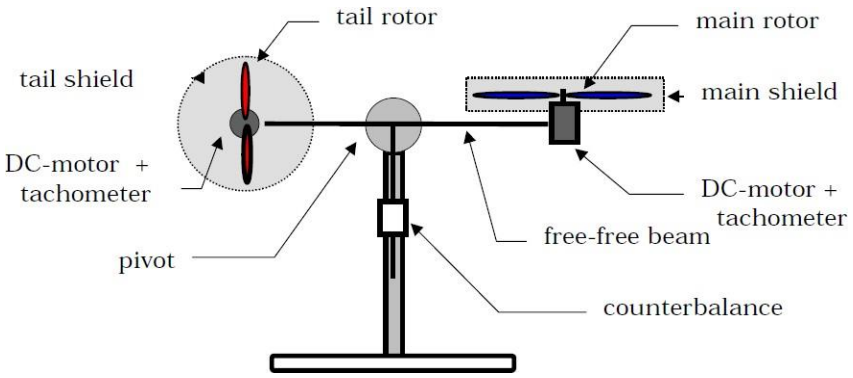

Figure 1. The Aero-dynamical model of the TRMS system [19]

$$\dot{s}_v = l_m S_f F_v(\omega_m) - {}_2 g(0.0099 \cos a_v + 0.0168 \sin a_v) - k_v \Omega_v - 0.0252 \Omega_h \sin 2a_v, \quad (2)$$

$$\dot{i}_h = \frac{1}{T_{tr}}(u_h - i_h), \quad (3)$$

$$\dot{i}_r = \frac{1}{T_{mr}}(u_v - i_v), \quad (4)$$

where

$$\Omega_h = \dot{a}_h = \frac{s_h + J_{mr}\omega_m(i_v)\cos a_v}{D \sin^2 a_v + E \cos^2 a_v + {}'G} \quad (5)$$

$$\Omega_v = \dot{a}_v = 9.1(s_v + J_{tr}\omega_t(i_t)), \quad (6)$$

$$\omega_m(i_r) = 90.99 i_v^6 + 599.73 i_v^5 - 129.26 i_v^4 - 1283.64 i_v^3 + 63.45 i_v^2 + 1283.41 i_v, \quad (7)$$

$$\omega_t(i_h) = 2020 i_h^5 - 194.69 i_h^4 - 4283.15 i_h^3 + 262.27 i_h^2 + 3768.83 i_h, \quad (8)$$

$$F_r(\omega_m) = -3.48 \times 10^{-12}\omega_m^5 + 1.09 \times 10^{-9}\omega_m^4 + 4.123 \times 10^{-6}\omega_m^3 - 1.632 \times 10^{-4}\omega_m^2 + 9.544 \times 10^{-2}\omega_m \quad (9)$$

and

$$F_h(\omega_t) = -3 \times 10^{-14}\omega_t^5 - 1.595 \times 10^{-11}\omega_t^4 + 2.511 \times 10^{-7}\omega_t^3 - 1.808 \times 10^{-4}\omega_t^2 + 8.01 \times 10^{-2}\omega_m. \quad (10)$$

Armature currents of the main and tail propellers are represented by i_r and i_h separately. ω_m and ω_t are further used to represent angular velocity of the main and tail propellers; while F_v and F_h represent the propulsive forces that move the system's join beam in the vertical and

Table 1. The coefficients of TRMS [19].

Symbol	Definition	Value
l_m	main part length of beam	0.236 m
l_t	tail part length of beam	0.25 m
k_v	friction coefficient for vertical axis	0.0095
k_h	friction coefficient for horizontal axis	0.0054
J_{mr}	moment of inertia in the DC-Motor of main propeller	$1.6543 \times 10^{-5} kgm^2$
J_{tr}	moment of inertia in the DC-Motor of tail propeller	$2.65 \times 10^{-5} kgm^2$
T_{mr}	time constant of main rotor	1.432 s
T_{tr}	time constant of tail rotor	0.3842 s
D	mechanical related constant	$1.6065 \times 10^{-3} kgm^2$
E	mechanical related constant	$4.90092 \times 10^{-2} kgm^2$
G	mechanical related constant	$6.3306 \times 10^{-3} kgm^2$
S_f	balance scale	8.43318×10^{-4}
g	gravitational acceleration	$9.81\ m/s^2$

horizontal directions. Angular momentums for both the horizontal and vertical planes are then denoted by s_h and s_v, respectively. With this, detailed coefficients are thoroughly outlined in Table 1. Following this, let's consider the neuroendocrine-PID controller implemented within the previously mentioned TRMS system as shown in Fig. 2, where $r_1(t)$ and $r_2(t)$ are the desired references, $u_1(t) = u_h$ and $u_2(t) = u_v$ are the control voltage inputs for the independent DC-motors, and $y_1(t) = a_h$ and $y_2(t) = a_v$ being the output measurements. $G(s)$ represents the TRMS system, while ts is the sampling time for $t = 0,\ t_s,\ 2t_s,\ 3t_s \ldots Nt_s$, with N being the number of samples. Breaking down, neuroendocrine-PID is an integration between the PID controller, $C_{11}(s)$ and $C_{22}(s)$, and neuroendocrine, $E_{11}(e_1(t),\ \Delta h_{11})$ and $E_{22}(e_2(t),\ \Delta h_{22})$. First off, the PID controller is described as follows:

$$C_{11}(s) = K_{P11}\left(1 + \frac{1}{K_{I11}s} + \frac{K_{D11}s}{1 + (K_{D11}/N_{11})s}\right) \tag{11}$$

and

$$C_{22}(s) = K_{P22}\left(1 + \frac{1}{K_{I22}s} + \frac{K_{D22}s}{1 + (K_{D22}/N_{22})s}\right) . \tag{12}$$

where $K_{P\ 11}$ and $K_{P\ 22}$ are the proportional gains, K_{I11} and K_{I22} are the integral gains, K_{D11} and K_{D22} are the derivative gains, while N_{11} and N_{22} are the filter coefficients. The outputs of $C_{11}(s)$ and $C_{22}(s)$ are, thus, individually represented by $h_{11}(t) = C_{11}(s)e_1(t)$ and $h_{22}(t) = C_{22}(s)e_2(t)$. This further accounts for errors within the control system as illustrated in Fig. 2, which are understood as $e_1(t) = r_1(t)\ y_1(t)$ and $e_2(t) = r_2(t)\ y_2(t)$, respectively. Subsequently, the neuroendocrine gain is written as follows:

$$E_{11}(e_1(t),\ \Delta h_{11}(t)) = \alpha_{11}\left(\frac{(|\Delta h_{11}(t)|)^{\zeta_{11}}}{\lambda_{11} + ((|\Delta h_{11}(t)|)^{\zeta_{11}})} + \beta_{11}\right) L_{111} L_{211} \tag{13}$$

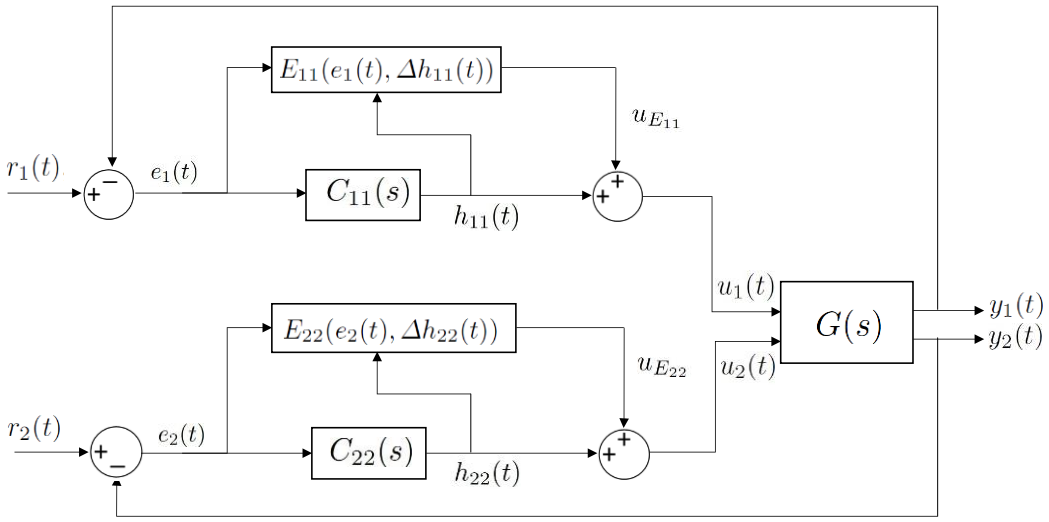

Figure 2. The Neuroendocrine-PID control system of TRMS

and

$$E_{22}(e_2(t),\ \Delta h_{22}(t)) = a_{22}\ \frac{(|\Delta h_{22}(t)|)^{\zeta_{22}}}{\lambda_{22} + ((|\Delta h_{22}(t)|)^{\zeta_{22}})} + \beta_{22}\ L_{122} L_{222} \tag{14}$$

where

$$L_{1_{11}} = -\frac{e_1(t)\ \ \Delta e_1(t)}{|e_1(t)|\ |\Delta e_1(t)|}, \quad L_{1_{11}} = \frac{\Delta h_{11}(t)}{|\Delta h_{11}(t)|} \tag{15}$$

and

$$L_{1_{22}} = -\frac{e_2(t)\ \ \Delta e_2(t)}{|e_2(t)|\ |\Delta e_2(t)|}, \quad L_{2_{22}} = \frac{\Delta h_{22}(t)}{|\Delta h_{22}(t)|} \tag{16}$$

such that $\Delta h_{11}(t) = h_{11}(t) - h_{11}(t - t_s)$ and $\Delta h_{22}(t) = h_{22}(t) - h_{22}(t - t_s)$ are the variance of $h_{11}(t)$ and $h_{22}(t)$, respectively. The change of error, $\Delta e_1(t) = e_1(t) - e_1(t - t_s)$, $\Delta e_2(t) = e_2(t) - e_2(t - t_s)$, as well as the parameters, $a_{11}, a_{22}, \beta_{11}, \beta_{22}, \lambda_{11}, \lambda_{11}, \zeta_{11}$ and ζ_{22} are hereby known to be positive real numbers. Note that, $E_{11}(e_1(t),\ \Delta h_{11}(t)) = 0$ and $E_{22}(e_2(t),\ \Delta h_{22}(t)) = 0$ would be fulfilled if $\Delta h_{11}(t) = 0$ and $\Delta h_{22}(t) = 0$, so β_{11} and β_{22} equal to 0 [20]. Furthermore, the direction factors executed for the purpose of effective error reduction are denoted by L_{111}, L_{211}, L_{122} and L_{222} through managing directions of the neuroendocrine gain in attaining a value of either 1 or -1.

Following this, the output neuroendocrine controller are explained as $E_{11}(e_1(t),\ \Delta h_{11}(t)) = u_{E11}$ and $E_{22}(e_2(t),\ \Delta h_{22}(t)) = u_{E22}$, respectively. Derived upon, outputs of the neuroendocrine-PID controller are hereby written as:

$$u_1(t) = h_{11}(t) + u_{E11} \tag{17}$$

and

$$u_2(t) = h_{22}(t) + u_{E22}. \tag{18}$$

Now, investigation would be focused on the operation as described in Fig. 2, with the following equations as a basis:

$$\bar{e}_j := \int_{t_0}^{t_f} |(r_j(t) - y_j(t)|^2 dt, \tag{19}$$

$$\bar{u}_i := \int_{t_0}^{t_f} |u_i)(t)|^2 dt, \tag{20}$$

where $r_j(t)$, $y_j(t)$ and $u_j(t)$ where $j = 1, 2$ and $i = 1, 2$. Moreover, the duration taken in evaluating the system's performance is being denoted with the time interval $[t_0, t_f]$, through which $t_0 \in \{0\} \cup \mathrm{R}_+$ and $t_f \in \mathrm{R}_+$. Nevertheless, the system's objective function is then written as:

$$J(\boldsymbol{K_P}, \boldsymbol{K_I}, \boldsymbol{K_D}, \boldsymbol{N}, \boldsymbol{\alpha}, \boldsymbol{\zeta}, \boldsymbol{\lambda}) = w_1\bar{e}_1 + w_2\bar{e}_2 + w_3\bar{u}_1 + w_4\bar{u}_2 \tag{21}$$

in which parameters are defined, with $\boldsymbol{K_P} := [K_{P\ 11}, K_{P\ 22}]$, $\boldsymbol{K_I} := [K_{I11}, K_{I22}]$, $\boldsymbol{K_D} := [K_{D11}, K_{D22}]$, $\boldsymbol{N} := [N_{11}, N_{22}]$, $\boldsymbol{\alpha} := [\alpha_{11}, \alpha_{22}]$, $\boldsymbol{\zeta} := [\zeta_{11}, \zeta_{22}]$ and $\boldsymbol{\lambda} := [\lambda_{11}, \lambda_{22}]$. The system's designer hereby takes on the role in setting both the weighting outputs, w_1 and w_2, as well as the input coefficients, w_3 and w_4. Broken down, the right side of Equation (21) further describes consistency in tracking error and input energy control towards the system's control performance.

Problem 2.1. With the control system outlined in Fig. 2, control parameters for the proposed neuroendocrine-PID are to be obtained, in the case where the objective function, $J(\boldsymbol{K_P}, \boldsymbol{K_I}, \boldsymbol{K_D}, \boldsymbol{N}, \boldsymbol{\alpha}, \boldsymbol{\zeta}, \boldsymbol{\lambda})$ would be minimized with regards to $\boldsymbol{K_P}, \boldsymbol{K_I}, \boldsymbol{K_D}, \boldsymbol{N}, \boldsymbol{\alpha}, \boldsymbol{\zeta}$ and $\boldsymbol{\lambda}$; in accordance to the data acquired for the $u_1(t)$, $u_2(t)$, $y_1(t)$ and $y_2(t)$ measurements.

3. Design of Data-driven Neuroendocrine-PID Control

In seek of resolution to Problem 2.1, ASED algorithm used in tuning the control parameters of neuroendocrine-PID is sequentially presented within the current section. The operation for designing the proposed neuroendocrine-PID controller to minimize the control objective in Equation (21) is then presented.

3.1. Adaptive Safe Experimentation Dynamics Algorithm

Let's consider the optimization problem towards minimizing the objective function, $f(\boldsymbol{p})$ be:

$$\min_{\boldsymbol{p} \in \mathrm{R}^n} f(\boldsymbol{p}) \tag{22}$$

with $\boldsymbol{p}$ being the design parameter. The Adaptive Safe Experimentation Dynamics (ASED) algorithm [15] is, thus, implemented to obtain the optimal solution, $\boldsymbol{p}$ through continuous updates on the design parameter. Updated law of the ASED algorithm is hereby given as:

$$p_i(k+1) = \begin{cases} h(\bar{p}_i - K_g rv_2) + K_{g1} \frac{f(\boldsymbol{p}(k)) - \bar{f}}{f(\boldsymbol{p}(k))} & \text{if } rv_1 \le ET, \\ \bar{p}_i + K_{g1} \frac{f(\boldsymbol{p}(k)) - \bar{f}}{f(\boldsymbol{p}(k))} & \text{if } rv_1 > ET, \end{cases} \tag{23}$$

where $p_i \in \mathrm{R}$ represents the i^{th} element of design parameter, $\boldsymbol{p}$, and $k = 1, 2, \ldots, k_{\max}$ is the number of iteration. Herewith, $\bar{p}_i \in \mathrm{R}$ is used to represent the best present value of design parameters, which, similarly denotes the i^{th} element of $\bar{\boldsymbol{p}} \in \mathrm{R}^n$. Besides, the size of interval towards decision making with regards to the random steps in $p_i \in \mathrm{R}$ has been denoted by K_g; the adaptive coefficient is denoted by K_{g1}; while, a probability value $\boldsymbol{p}$ is represented by ET. The random number uniformly selected between 0 and 1, and the new random number selected

between $p_{\min}$ and $p_{\max}$ are hereby indicated through $rv_1 \in \mathsf{R}$ and $rv_2 \in \mathsf{R}$, independently. Subsequently, the function, $h(\bar{p}_i - K_g rv_2)$ from Equation (23)) is described as:

$$h(\cdot) = \begin{cases} p_{\max}, & \text{if } \bar{p}_i - K_g rv_2 < p_{\max}, \\ \bar{p}_i - K_g rv_2, & \text{if } p_{\min} \le \bar{p}_i - K_g rv_2 \le p_{\max}, \\ p_{\min}, & \text{if } \bar{p}_i - K_g rv_2 < p_{\min}. \end{cases} \tag{24}$$

with the predetermined values for maximum and minimum parameters being represented through the symbols, $p_{\max}$ and $p_{\min}$. Essentially, procedure in executing the ASED method has been outlined in Fig. 3.

3.2. Data-driven controller design

A logarithmic scale is hereby employed to the design parameter, $\boldsymbol{p}$ in enabling greater effectiveness towards gaining the optimal controller parameters. Incorporated upon, the parameters of neuroendocrine-PID are, thus, stated as:

$$\boldsymbol{\psi} = J(\boldsymbol{K_P}, \boldsymbol{K_I}, \boldsymbol{K_D}, \boldsymbol{N}, \boldsymbol{\alpha}, \boldsymbol{\zeta}, \boldsymbol{\lambda}) \in \mathsf{R}^n \tag{25}$$

where each element of $\boldsymbol{\psi}$ is given by $\psi_i = 10^{p_i} (i = 1, 2, \ldots, 14)$. Following this, the objective function is being written as $f(\boldsymbol{p}) = [10^{p_1}\ 10^{p_2} \ldots 10^{p_n}]^{\mathrm{T}}$. Under such circumstance, the procedure in designing neuroendocrine-PID tuned via the ASED method is described as follows:

Step 1: The objective function, $f(\boldsymbol{p}) = J(\boldsymbol{K_P}, \boldsymbol{K_I}, \boldsymbol{K_D}, \boldsymbol{N}, \boldsymbol{\zeta}, \boldsymbol{\lambda}, \boldsymbol{\alpha})$, and each design parameter, $p_i = \log \psi_i$ are initially determined. Next, the necessary maximum iteration, $k_{\max}$ was set.
Step 2: Optimal design parameters, as based on Equation (25), are obtained through the implementation of the ASED algorithm.
Step 3: Following the achievement of $k_{\max}$, the optimal design parameter, $\boldsymbol{p}_{\text{opt}} = \bar{\boldsymbol{p}}(k_{\max})$ is subsequently obtained. $\boldsymbol{\psi}_{\text{opt}} = [10^{p_{1\text{opt}}} \quad 10^{p_{2\text{opt}}} \quad \ldots \quad 10^{p_{14\text{opt}}}]^{\mathrm{T}}$ is then applied to $C_{11}(s)$, $C_{22}(s)$, $E_{11}(e_1(t), \Delta h_{11}(t))$ and $E_{22}(e_2(t), \Delta h_{22}(t))$ for the control system in Fig. 2.

4. Numerical Example

Within this section, numerical findings obtained on objective function, $J(\boldsymbol{K_P}, \boldsymbol{K_I}, \boldsymbol{K_D}, \boldsymbol{N}, \boldsymbol{\zeta}, \boldsymbol{\lambda}, \boldsymbol{\alpha})$, total norm of error, $\bar{e}_1 + \bar{e}_2$, and total norm of input, $\bar{u}_1 + \bar{u}_2$ were assessed in evaluating performance of the proposed controller for a TRMS system. As such, robustness of neuroendocrine-PID was analyzed alongside a standard PID, further determining its enhanced excellence to that of the previous controller. This was done by gauging the percentage of improvement in control accuracy, J_{obj} between the proposed and the standard PID controllers, through the calculation:

$$\%J_{obj} = \frac{|J_{NE} - J_{PID}|}{J_{PID}} \times 100\%. \tag{26}$$

Next, the TRMS system in Fig. 1 is considered, where are derived from Equations (1)-(10). Herewith, the desired positions were set as $r_1(t) = 0.5$ and $r_2(t) = 0.5$, respectively. The design parameters for the controller, $\boldsymbol{\psi} := [\boldsymbol{K_P}, \boldsymbol{K_I}, \boldsymbol{K_D}, \boldsymbol{N}, \boldsymbol{\zeta}, \boldsymbol{\lambda}, \boldsymbol{\alpha}] \in \mathsf{R}^{14}$ are further tabulated via Table 2. With the simulation interval, tf being pre-set at 60 s, and the total number of iteration, $k_{\max}$ being 1000; this activity aimed to obtain $\boldsymbol{\psi} \in \mathsf{R}^{14}$ that minimized the performance index, J as outlined in Equation (21), for $\omega_1 = 1000$, $\omega_2 = 1200$, $\omega_3 = 1$ and $\omega_4 = 1$. With this, coefficients for ASED were determined at $K_g = 0.022$, $K_{g1} = 0.0008$, $ET = 0.66$, . Based on the information in Table 2, preliminary experiments had been conducted prior to the simulation, in selecting the initial control parameters, $\boldsymbol{p}(0)$ of the proposed controller. Whereas,

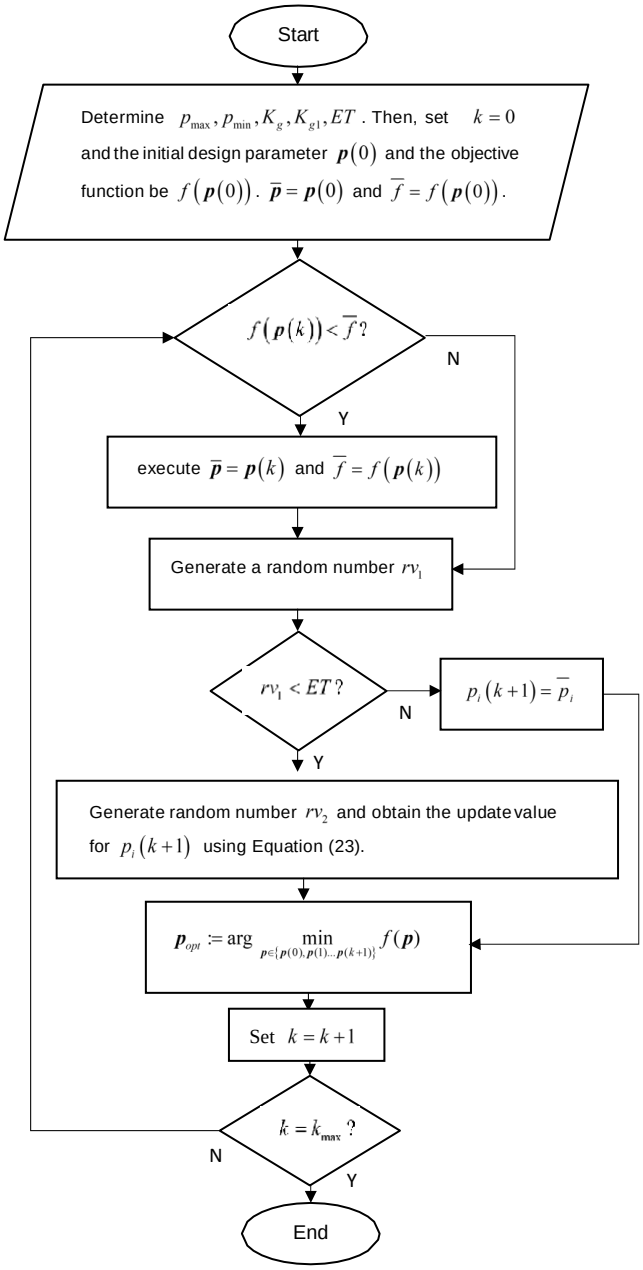

Figure 3. The ASED updated procedure

identical coefficients of the ASED method have also been applied in tuning the benchmarked standard PID, towards ensuring heightened practicality in the results obtained, under identical optimization conditions.

Following the simulation, the convergence curve for objective function, J with response to the ASED-based neuroendocrine-PID for the iteration, $k_{\max}$ = 1000 is illustrated in Fig. 4. Its downward sway hereby justified capability of the ASED-based method in minimizing the objective function, towards reaching the controller's optimal control parameters. Besides, output responses of the TRMS system, $y_1(t)$ and $y_2(t)$ through the implementation of neuroendocrine-PID and the standard PID controller are presented in Figs. 5 and 6, with their control input

Table 2. Neuroendocrine-PID controller parameters for TRMS system

ψ	Neuroendocrine-PID	$p(0)$	$10^{p(0)}$	p_{opt}	$10^{p_{opt}}$
ψ_1	$K_{P\,11}$	-0.8	0.2	-0.638	0.230
ψ_2	K_{I11}	2.9	794.3	3.783	6066.0
ψ_3	K_{D11}	-0.5	0.3	-0.054	0.883
ψ_4	N_{11}	1.7	50.1	2.275	188.45
ψ_7	a_{11}	0	1.0	-0.298	0.504
ψ_5	ζ_{11}	0	1.0	-0.263	0.546
ψ_6	λ_{11}	0	1.0	0.150	1.412
ψ_{17}	$K_{P\,22}$	-2.2	0.0	-2.492	0.003
ψ_{18}	K_{I22}	-2.8	0.0	-1.934	0.012
ψ_{19}	K_{D22}	2.7	501.2	2.825	668.34
ψ_{20}	N_{22}	4	10000	3.966	9236.3
ψ_{23}	a_{22}	0	1.0	0.755	5.687
ψ_{21}	ζ_{22}	0	1.0	0.107	1.280
ψ_{22}	λ_{22}	0	1.0	-1.176	0.067

responses, u_1 and u_2 being demonstrated in Fig. 7 and Fig. 8, respectively (i.e. neuroendocrine-PID, standard PID and reference lines are separately indicated with blue, red and black dotted lines). In comparison, neuroendocrine-PID is shown to generate better responses under the horizontal and vertical planes, $y_1(t)$ and $y_2(t)$; with a shorter overshoot recorded as compared to its standard counterpart. Yet, such performance excellence from the proposed controller seems to require a lower control energy inputs, u1(t) and u2(t), in controlling the TRMS system.

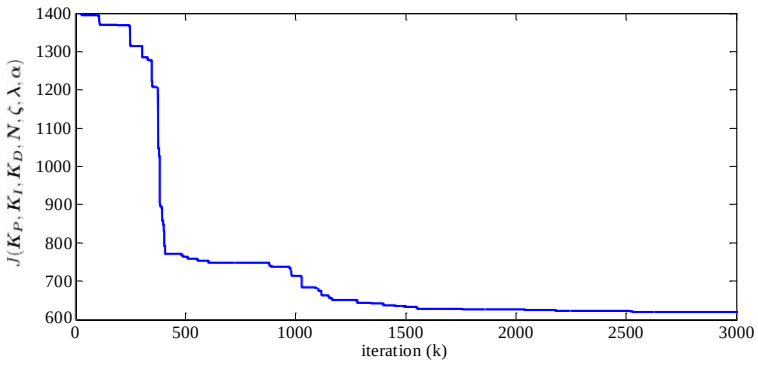

Figure 4. The objective function, $J(K_P, K_I, K_D, N, \zeta, \lambda, \alpha)$ for TRMS

To support the fore-discussed findings, numerical analysis on the objective function, J, total norm of error, $\bar{e}_1 + \bar{e}_2$, and total norm of input, $\bar{u}_1 + \bar{u}_2$ has been stated in Table 3. As shown, neuroendocrine-PID has yielded slightly lower values to that of its predecessor in the essential aspects assessed within the current study. Not to mention, a 13.2 % improvement has been obtained through the proposed controller in term of control accuracy, following the calculation

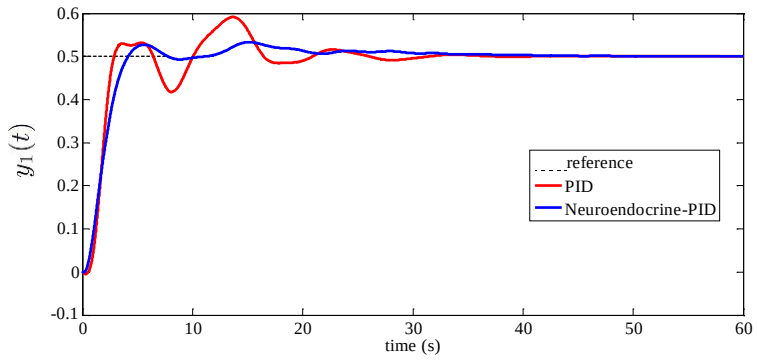

Figure 5. horizontal plane $y_1(t)$ responses

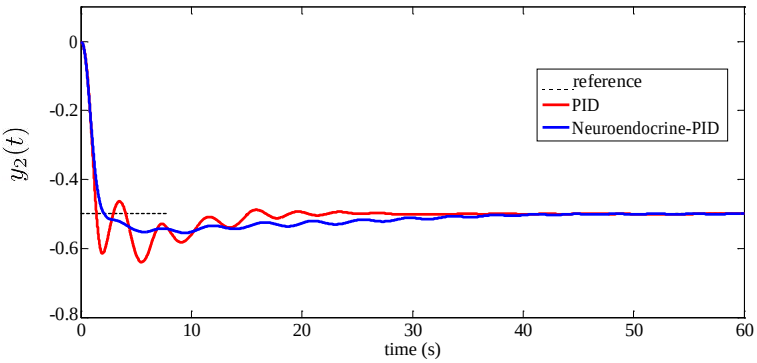

Figure 6. vertical plane $y_2(t)$ responses

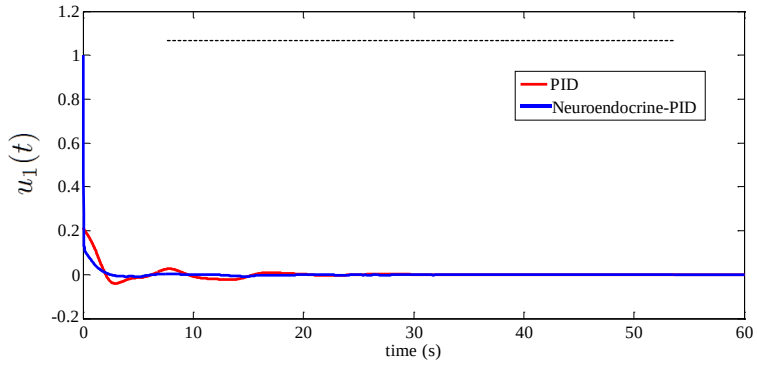

Figure 7. Input $u_1(t)$ responses

outlined in Equation (26). The significance of neuroendocrine gain in contributing to better control of TRMS systems is, thus, confirmed.

5. Conclusion

This paper explores implementation of the neuroendocrine-PID controller on TRMS systems, tuned through the ASED method. With the generation of effective extra gain, neuroendocrine has demonstrated significance towards improved control accuracy. Smaller objective function,

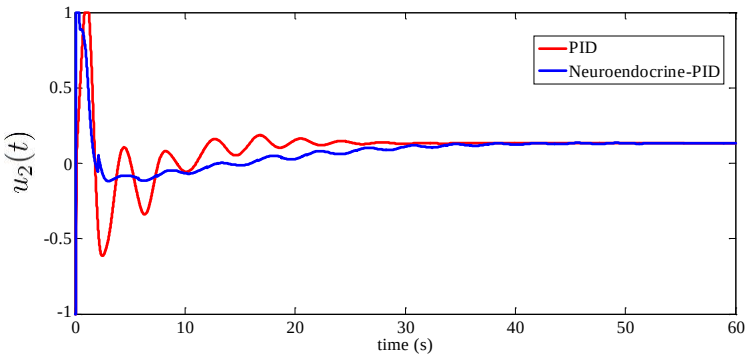

Figure 8. Input $u_2(t)$ responses

Table 3. Numerical result of container gantry crane system

Controller	PID	Neuroendocrine-PID
J	712.55	**618.14**
$\bar{e}_1 + \bar{e}_2$	0.6291	**0.5662**
$\bar{u}_1 + \bar{u}_2$	37.1565	**9.1339**

total norm error, and total norm input of the proposed controller has hereby demonstrated greater robustness, specifically towards outperforming its predecessor, the standard PID controller, in term of control performance accuracy. This is shown via a recorded improvement of 13.2 % in control accuracy following the implementation of neuroendocrine-PID, as compared to the standard PID controller.

6. Acknowledgement

Completion of this research is credited to the prodigious support from the Ministry of Higher Education, under *Skim Latihan Akademik Bumiputra* (SLAB); as well as the financial aid given by the Post Graduate Research Grant (PGRS-180349) by Universiti Malaysia Pahang.

References

[1] Biswas P, Maiti R, Kolay A, Sharma K D and Sarkar G 2014 Pso based pid controller design for twin rotor mimo system *Proceedings of The 2014 International Conference on Control, Instrumentation, Energy and Communication (CIEC)* (IEEE) pp 56–60

[2] Juang J G, Huang M T and Liu W K 2008 *IEEE Transactions on Systems, Man, and Cybernetics, Part C (Applications and Reviews)* **38** 716–727

[3] Sivadasan J and Willjuice Iruthayarajan M 2018 *Tehnički vjesnik* **25** 105–111

[4] Pandey S K, Dey J and Banerjee S 2018 Design of h infinity$_\infty$ controller for twin rotor mimo system (trms) based on linear matrix inequalities *Advanced Computational and Communication Paradigms* (Springer) pp 465–473

[5] Pandey S K and Laxmi V 2015 Optimal control of twin rotor mimo system using lqr technique *Computational Intelligence in Data Mining-Volume 1* (Springer) pp 11–21

[6] Hashim H A and Abido M A 2015 *Computational intelligence and neuroscience* **2015** 49

[7] Mahmoud T S, Marhaban M H and Hong T S 2010 *IEEJ Transactions on Electrical and Electronic Engineering* **5** 369–371

[8] Faris F, Moussaoui A, Djamel B and Mohammed T 2017 *Proceedings of the Institution of Mechanical Engineers Part I Journal of Systems and Control Engineering* **231** 3–13

[9] Zeghlache S and Amardjia N 2018 *Optik* **156** 391–407

[10] Ahmad M A, Azuma S i and Sugie T 2014 *Expert Systems with Applications* **41** 6361–6370

[11] Ahmad M A, Mustapha N M Z A, Nasir A N K, Tumari M Z M, Ismail R M T R and Ibrahim Z 2018 Using normalized simultaneous perturbation stochastic approximation for stable convergence in model-free control scheme *2018 IEEE International Conference on Applied System Invention (ICASI)* (IEEE) pp 935–938

[12] Sugumaran G, Vinothkumar L, Isvariya A and Janardhanan M 2015 *International Journal on Applications in Electrical and Electronics Engineering* **1** 32–35

[13] Ghazali M R, Ahmad M A, Jusof M F M and Ismail R M T R 2018 A data-driven neuroendocrine-pid controller for underactuated systems based on safe experimentation dynamics *Signal Processing & Its Applications (CSPA), 2018 IEEE 14th International Colloquium on* (IEEE) pp 61–66

[14] Ghazali M R, Ahmad M A and Ismail R M T R 2018 Data-driven neuroendocrine-pid tuning based on safe experimentation dynamics for control of tito coupled tank system with stochastic input delay *International Conference on Robot Intelligence Technology and Applications* (Springer) pp 1–12

[15] Ghazali M R b, Ahmad M A b and Raja Ismail R M T b 2019 *IETE Journal of Research* 1–14

[16] Feng J and Shen W Z 2015 *Renewable Energy* **78** 182–192

[17] Ding Y, Chen L and Hao K 2018 Human body based intelligent cooperative decoupling controllers *Bio-Inspired Collaborative Intelligent Control and Optimization* (Springer) pp 25–80

[18] Ghazali M R, Ahmad M A, Raja Ismail R M T and Tokhi M O 2019 *Journal of Low Frequency Noise, Vibration and Active Control* 1461348419867524

[19] Twin Rotor M 1998 *Feedback Instruments Ltd, Crowborough, UK*

[20] Ding Y, Xu N, Ren L and Hao K 2015 *IEEE Trans. Contr. Sys. Techn.* **23** 1205–1212